AGU PUBLICATIONS

JGR

Journal of Geophysical Research: Oceans

RESEARCH ARTICLE
10.1002/2014JC010109

Special Section:
Early scientific results from the salinity measuring satellites Aquarius/SAC-D and SMOS

Comparison of spaceborne measurements of sea surface salinity and colored detrital matter in the Amazon plume

S. Fournier[1], B. Chapron[1], J. Salisbury[2], D. Vandemark[2], and N. Reul[1]

[1]Laboratoire d'Océanographie Spatiale, Ifremer, Brest, France, [2]Ocean Processes Analysis Laborator University of New Hampshire, Durham, New Hampshire, USA

Key Points:
- First time mapping of ocean color/SSS at high spatiotemporal resolution
- In situ/satellite comparisons of the conservative mixing relationship
- Improved method to reconstruct SSS field back in time

Correspondence to:
S. Fournier,
severine.fournier@ifremer.fr

Citation:
Fournier, S., B. Chapron, J. Salisbury, D. Vandemark, and N. Reul (2015), Comparison of spaceborne measurements of sea surface salinity and colored detrital matter in the Amazon plume, *J. Geophys. Res. Oceans*, *120*, 3177–3192, doi:10.1002/2014JC010109.

Received 2 MAY 2014
Accepted 10 MAR 2015
Accepted article online 16 MAR 2015
Published online 2 MAY 2015

Abstract Large rivers are key hydrologic components in oceanography, particularly regarding air-sea and land-sea exchanges and biogeochemistry. We enter now in a new era of Sea Surface Salinity (SSS) observing system from Space with the recent launches of the ESA Soil Moisture and Ocean Salinity (SMOS) and the NASA Aquarius/Sac-D missions. With these new sensors, we are now in an excellent position to revisit SSS and ocean color investigations in the tropical northwest Atlantic using multiyear remote sensing time series and concurrent in situ observations. The Amazon is the world's largest river in terms of discharge. In its plume, SSS and upper water column optical properties such as the absorption coefficient of colored detrital matter (a_{cdm}) are strongly negatively correlated (<-0.7). Local quasi-linear relationships between SSS and a_{cdm} are derived for these plume waters over the period of 2010–2013 using new spaceborne SSS and ocean color measurements. Results allow unprecedented spatial and temporal resolution of this coupling. These relationships are then used to estimate SSS in the Amazon plume based on ocean color satellite data. This new product is validated against SMOS and in situ data and compared with previously developed SSS retrieval models. We demonstrate the potential to estimate tropical Atlantic SSS for the extended period from 1998 to 2010, prior to spaceborne SSS data collection.

1. Introduction

Large rivers are key components of the global water cycle, and their discharge into the ocean plays an important role in several physical, biological, optical, and chemical ocean processes. Freshwater inputs into the open ocean modify the local sea surface salinity (SSS) and therefore the buoyancy and vertical stratification of the surface layers [*Pailler et al.*, 1999; *Masson and Delecluse*, 2001; *Ferry and Reverdin*, 2004]. They also provide organic and inorganic particulates into the ocean, impacting biogeochemical and ecological activity [*McKee et al.*, 2004; *Hickey et al.*, 2010]. Being able to routinely monitor the dispersal patterns of river plumes, their spatial extension and mixing rates, is an important goal to support a better understanding of these processes.

Today, sea surface salinity (SSS) observations are available from the ESA Soil Moisture and Ocean Salinity (SMOS) and the NASA Aquarius/SAC-D satellite missions. SMOS and Aquarius measurements now provide unprecedented mapping capabilities at improved spatiotemporal resolution. The SMOS revisit time at the Equator is about 3 days and the spatial resolution is 43 km. Aquarius provides global coverage every 7 days and its spatial resolution is about 100 km. With satellite SSS now available, this enables a more in depth examination of the spatiotemporal behavior of coincident colored detrital matter and salinity over the Amazon plume.

Salinity change caused by mixing of adjacent water masses can be considered as a conservative property of water masses [*Tomczak*, 1999], as there is no significant source or sink of salt in the ocean interior. Ocean-atmosphere fluxes thus are neglected over this area, as the precipitation rate represents less than 10% of the freshwaters supplied by the Amazon River [*Lentz and Limeburner*, 1995]. Assuming that dilution is the sole mixing process, salinity tends to increase linearly as fresh waters mix into the saltier open ocean. In these conditions, riverine constituent concentration also tends to decrease proportionally to salinity changes. Oceanic water properties that undergo dilution are considered to follow a conservative mixing assumption. Accordingly, a strong negative linear correlation between sea surface salinity and biological, chemical, and optical parameters is often reported for numerous river estuaries [*Ferrari and Dowell*, 1998; *Binding and Bowers*, 2003; *Hu et al.*, 2003; *Chen et al.*, 2007; *Granskog et al.*, 2007; *Bowers and Brett*, 2008; *Del*

Castillo and Miller, 2008; *Urquhart et al*., 2012; *Bai et al*., 2013] (e.g., *Del Vecchio and Subramaniam* [2004] reports $R^2 = 0.93$ between sea surface salinity and light absorption at 490 nm). This linear SSS-riverine constituents relationship can vary significantly [*Blough and Del Vecchio*, 2002]. The variation of riverine constituent concentration at river mouths is indeed a function of hydrology and land cover attributes for a given river [*Battin*, 1998; *Salisbury*, 2003; *Huang and Chen*, 2009; *Salisbury et al*., 2008]. Both vary geographically and seasonally, and can exhibit time scales of variability that depend on accumulated rainfall upstream. In addition, departures from the linear conservative mixing may occur due to physical and chemical processes downstream of the mouth. These include mixing with additional water masses [*Blough and Del Vecchio*, 2002] or in situ subsidies of river constituents released via net phytoplankton growth [*Twardowski and Donaghay*, 2001; *Yamashita and Tanoue*, 2004], microbial utilization [*Moran et al*., 1999; *Obernosterer and Herndl*, 2000], or photochemical oxidation [*Miller and Zepp*, 1995].

Within the Amazon and Orinoco plumes, relationships between SSS and colored detrital matter (cdm), chlorophyll concentration, and dissolved organic carbon have already been extensively studied [*Del Vecchio and Subramaniam*, 2004; *Hu et al*., 2004; *Molleri et al*., 2010; *Salisbury et al*., 2011]. The Amazon river discharges about 15% of the global freshwater runoff [*Baumgartner and Reichel*, 1975] with a strong seasonal variation reaching a maximum of about 2.4×10^5 m^3/s in mid-May and a minimum of 0.8×10^5 m^3/s in mid-November [*Lentz*, 1995]. It also supplies the largest riverine flux of suspended (1200 Mt yr^{-1}) and dissolved matter (287 Mt yr^{-1}) to the global ocean, which includes Colored Dissolved Organic Matter (CDOM) [*Meybeck and Ragu*, 1997]. Including the Orinoco River, which has the fourth largest river discharge on the planet, 20% of the global freshwater runoff enters the northwestern tropical Atlantic (NWTA). These river plumes have been tracked in the tropical Atlantic Ocean to more than 1000 km from shore [*Muller-Karger et al*., 1988; *Hu et al*., 2004]. They are fresher and warmer than the adjacent ocean, highly concentrated in dissolved and suspended matter, and have a key impact on the biogeochemical processes (sink for atmospheric CO_2 [*Körtzinger*, 2003]), optical properties [*Muller-Karger et al*., 1988; *Longhurst*, 1995; *Muller-Karger et al*., 1995; *Fratantoni and Glickson*, 2002; *Del Vecchio and Subramaniam*, 2004; *Hu et al*., 2004], ecology [*Muller-Karger et al*., 1995], and physical properties [*Masson and Delecluse*, 2001; *Mignot et al*., 2012].

Optical properties can be estimated either from spaceborne or in situ sensors. Two examples are absorption coefficient of colored detrital matter (a_{cdm}), at several wavelengths (355, 400, and 443 nm), and diffuse attenuation coefficient at 490 nm (K490). *Hu et al*. [2004] found $SSS = 38.18–118.24\ a_{CDOM}(400\ nm)$, using about 40 samples of colocalized S-PALACE floats SSS measurements and satellite CDOM values, acquired during two winter months in 1999. Based on CTD and in situ optical measurements along several ship transects, *Del Vecchio and Subramaniam* [2004] found different linear relationships between SSS and K490 depending on the location within the plume (proximity of the Amazon mouth or ~1000 km north-west off the latter). *Del Vecchio and Subramaniam* [2004] also investigated the relationship between SSS and CDOM absorption at 355 nm. During the low flow period (winter), no clear dependence on salinity was found. During the high flow period (spring), CDOM absorption at 355 nm decreased with increasing salinity for inshore waters along the river plume. Combining in situ SSS and the NASA Sea-viewing Wide Field-of-view Sensor (SeaWIFS) optical data, *Molleri et al*. [2010] determined the relationship ($SSS = -126.03\ a_{cdm}(443\ nm) + 37.259$), from 30 colocalized samples at oceanographic stations in the proximity of the Amazon mouth, acquired at different periods of the seasonal cycle between 1999 and 2003. Finally, *Salisbury et al*. [2011] studied the spatial coherence between the Amazon discharge, cdm absorption and SSS, and the nature of the SSS-a_{cdm} relationship using spaceborne estimates of sea surface salinity deduced from the AMSR-E instrument [*Reul et al*., 2009].

The objective of this present study is to employ the newly available SMOS SSS data in conjunction with standard optical products, to more thoroughly document relationships between sea surface salinity and colored detrital matter in the Amazon plume at finer time and spatial scales. The correlation between SSS and optical properties in the Amazon plume is studied from 2010 to 2013 using remote sensing data to investigate its spatiotemporal variability. A methodology to map SSS in the Amazon plume from ocean color data is then proposed to map SSS back in time, from 1998 to 2013.

2. Data

We use sea surface salinity data from the SMOS mission. The Level-3 gridded 0.25° resolution SMOS SSS data were obtained from the Ocean Salinity Expertise Center (CECOS) of the CNES-IFREMER Centre Aval de

Traitement des Données SMOS (CATDS) (http://catds.ifremer.fr). We use daily products averaged with a 10 day running mean, reprocessed in 2012. Due to land contamination, the first three pixels from the coast are discarded, i.e., excluding data within 150 km of the coast. Overall accuracy of the 10 day composite products at 25 km resolution is on the order of 0.3 practical salinity scale (pss) in the tropical oceans [*Reul et al*., 2013; *Fournier*, 2014].

We use the level 3 daily, 4 km resolution estimates of optical parameters processed and distributed by ACRI-ST GlobColour service (http://www.globcolour.info/). We specifically use the absorption coefficient of colored detrital matter at 443 nm (a_{cdm}). This product is spatially interpolated at 25 km and it is resampled with a 10 day running mean. The product used in this study is based on the Garver, Siegel, and Maritorena (GSM) model [*Maritorena et al*., 2002]. Over the global world ocean, this product shows a good agreement with in situ data (rms = 0.14) [*Maritorena et al*., 2002]. Nevertheless, it is expected that errors in a_{cdm} could be considerably greater in waters with high sediment concentrations [*Salisbury et al*., 2011].

Daily and monthly discharge data of Amazon and Orinoco rivers, at the Obidos and Bolivar gauging stations, respectively, were obtained from the Environmental Research Observatory Geodynamical, Hydrological, and Biogeochemical control of erosion/alteration and material transport in the Amazon basin (ORE-HYBAM), available at http://www.ore-hybam.org/.

In situ sea surface salinity observations are used to validate our SSS retrieval model from ocean color. We use the 5 m depth salinity data transects acquired in the Amazon-Orinoco River plume region during 2010–2012 from the ThermoSalinoGraph (TSG) sensors onboard ships of opportunity and gathered during the Global Ocean Surface Underway Data (GOSUD) project. These include data from transects regularly acquired along a Europe-French Guiana shipping route collected by vessels *Colibri* and *Toucan*. We considered a collection of underway TSG SSS measurements at 3 m depth collected from also the *R/V Knorr* during several cruises in 2010 across the Amazon River plume. Comparing in situ measurements with SMOS SSS measurements raises issues considering the differences in the respective spatiotemporal sampling characteristics of the space and in situ sensors. An overall bias on the order of 0.3–0.5 pss is obtained that is in-line with open ocean comparisons. Yet, a generally higher standard deviation of the satellite/in situ SSS differences ($\sim$1 pss for SSS $<$ 35 pss) is found in the plume waters. This is not unexpected given the high horizontal and vertical spatiotemporal variability [*Reul et al*., 2012; *Fournier*, 2014].

The 16 km 8 day Carbon-based Production Model (CbPM) Net Primary Productivity (NPP) products from Ocean Productivity were used. Such data are available on their website (http://www.science.oregonstate.edu/ocean.productivity/). These products have been averaged at the SMOS product 25 km resolution. CbPM data used here are based on the updated model by *Westberry et al*. [2008].

Finally, we use data from the 6.9 and 10.7 GHz frequency bands of the Advanced Microwave Scanning Radiometer-EOS (AMSR-E) onboard NASA EOS Aqua satellite. The spatial resolution of the instrument is 38 km in the C-band (6.9 GHz) and 56 km in the X-band (10.7 GHz). We specifically apply the L2A and L2B brightness temperature products resampled at 56 km spatial resolution from the National Snow and Ice Data Center (NSIDC) (http://nsidc.org/data/). The revisit time of the platform Aqua is about 1–2 days. This along-track product is spatially interpolated at 25 km and it is resampled with a 10 day running mean, as done for SMOS data.

3. Correlations Between SSS and Optical Properties

Spatial and temporal SSS variability from 2010 to 2013 for the northwestern tropical Atlantic (NWTA) region are provided in the mean monthly SMOS maps shown in Figure 1. The plume waters, fresher than 35.5 pss, are spreading from the Amazon mouth to the open ocean further than 1000 km from the mouth, northwestward, or eastward. To delimit the Amazon plume, the 35.5 pss value has been chosen as a threshold to extract river plume waters from the open ocean. While somewhat arbitrary, 35.5 pss represents an inflection point at which SSS and a_{cdm} no longer covary. A map of the correlations between daily $\pm$5 days SMOS SSS and a_{cdm} over 2010–2013 is presented in Figure 2. At each 0.25 $\times$ 0.25° grid point, the correlation between SMOS SSS and ocean color time series is evaluated, and only pixels for which the *p*-value (significance of the SSS-a_{cdm} correlation) is below 0.01 are shown. A strong negative correlation (below $-$0.5) between SMOS SSS and a_{cdm} is obtained inside the river plume delimited by the 35.5 pss contour. The largest

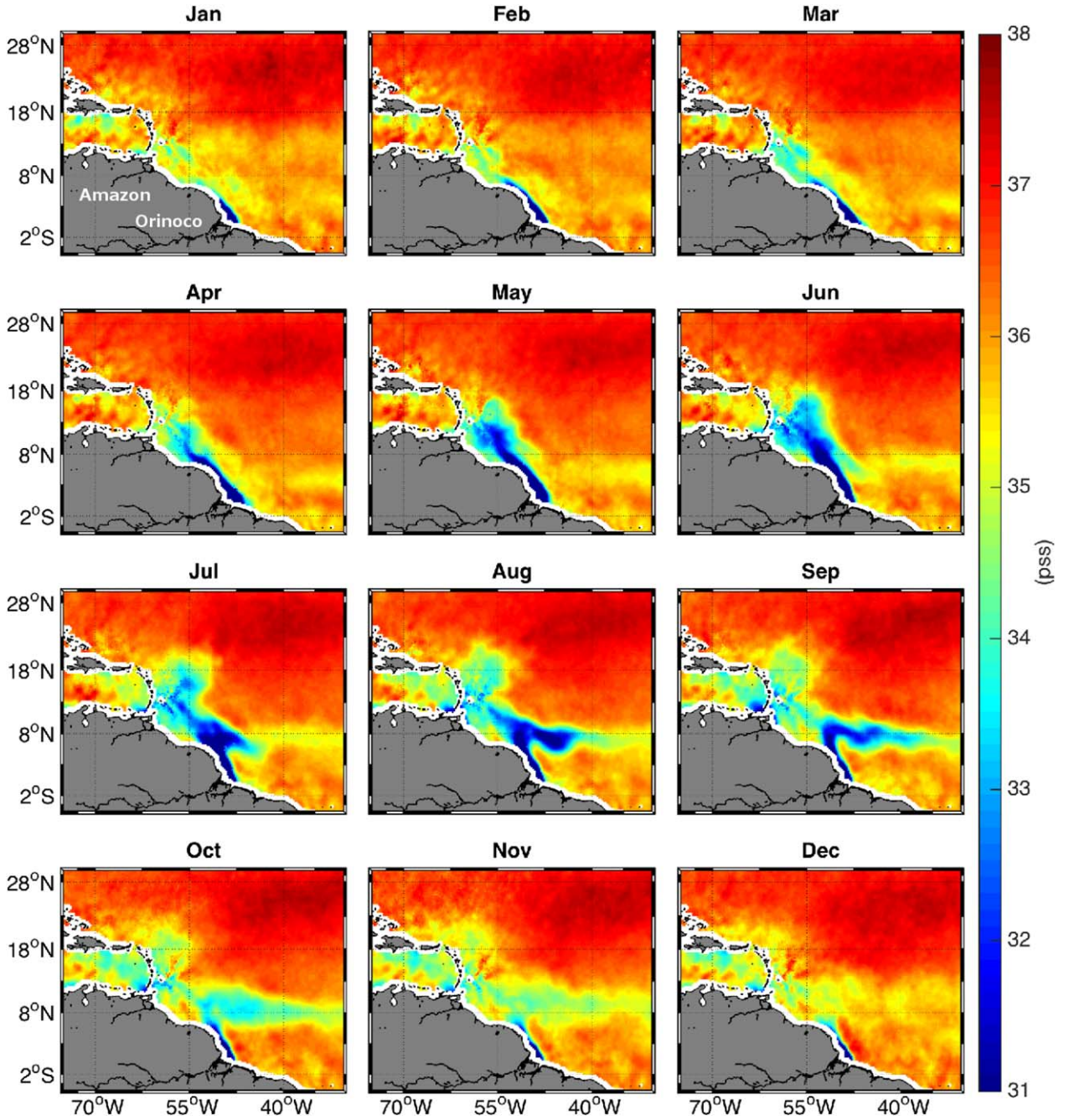

Figure 1. The 2010–2013 monthly mean SMOS SSS maps.

negative correlations between SMOS SSS and a_{cdm} (below −0.95) are found in the eastern part of the plume (pointed out by a black dot).

Monthly time series of SMOS sea surface salinity and a_{cdm} at three NWTA locations [6.5°N 46°W], [14°N 55°W], and [19°N 51.5°W] (labeled as 1, 2, and 3 in Figure 2) are shown in Figure 3. In the Amazon plume area, a seasonal cycle is clearly observed in accordance with the Amazon River discharge cycle. Once per year, as Amazon waters reach a given area, SSS locally drops below 35 pss and the a_{cdm} increases.

In the eastern part of the plume, the SMOS SSS varies between approximately 30–31 pss, in August, and 36 pss (outside of the plume), from February to May. The monthly mean a_{cdm} in this area varies between

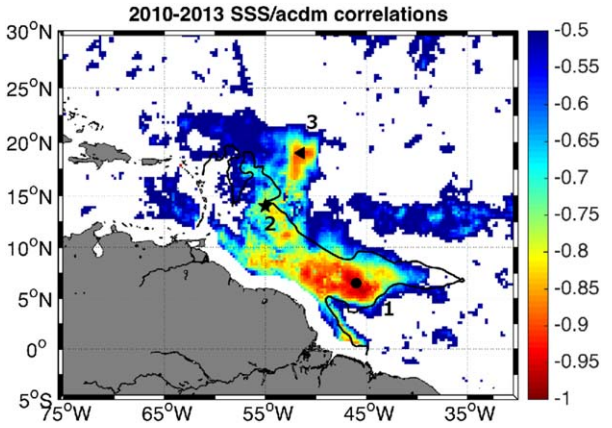

Figure 2. Correlation between daily ±5 days SMOS SSS and a_{cdm} for each 0.25 × 0.25° pixel. Only *p*-values (significance of the correlation) below 0.01 are shown. The square, pentagram, and triangle (labeled 1, 2, and 3) are representing the pixels with coordinates: [6.5°N 46°W], [14°N 55°W], and [19°N 51.5°W], respectively. The black thick line is the average location of the plume delimited by the 35.5 pss contour.

0.01 m^{-1}, during winter and spring, and 0.06–0.08 m^{-1} in August. In the northwestern part of the plume, the SMOS SSS evolves between 32 and 33 pss in June–August, and 36 and 37 pss from October to April. The monthly mean a_{cdm} peaks in June–August when the minimum SSS is reached.

As the extension of the plume varies from year to year, strong negative correlations (below −0.85) are also found outside the average plume contour (shown by a red dot in Figure 2). There SMOS SSS is quasi constant, around 36–37 pss and a_{cdm}, around 0.005–0.01 m^{-1}. Only one anomalous event in July 2011 occurs, during which SMOS SSS dropped to 33 pss while a_{cdm} increased to 0.03 m^{-1} (see Figure 3c). The plume reaching this area during the 2011 summer is also confirmed with Aquarius data [*Grodsky et al*., 2014]. SSS and a_{cdm} are strongly synchronized at these three locations and more generally over the whole plume region.

At the Obidos gauge, the Amazon discharge is maximal around June–July with a discharge of about 2.5 × 10^5 m^3/s, and at its minimum around October–November with a discharge of approximately 0.5–1 × 10^5 m^3/s (see Figure 3d). SSS and a_{cdm} signals are clearly related to the Amazon discharge cycle. In the eastern area of the plume, lags of about 2–3 months are found between the maximum discharge level and the minimum SSS or the maximum a_{cdm} (see Figures 3a and 3d). As found (not shown), the highest correlations are near −0.7, for a time lag of 3 months. In the northwestern part of the plume, the discharge and SSS signals and the discharge and a_{cdm} signals are correlated, around −0.6, with no time lag (see Figures 3b and 3d) because Amazon waters rapidly and continuously reach this area to influence the ambient sea surface properties.

Typically Amazon plume waters reach each location at different periods of the year. The seasonal variability of the plume in the northwestern tropical Atlantic is mapped in Figure 4 (red patterns in Figure 4 indicate a_{cdm} maximum occurrence for each pixel). The signal extrema (SSS minimum, a_{cdm} maximum) occur when the Amazon influence is largest: near the river mouth in April; in the northwestern part of the plume around June–July; and in the northern areas—around August–October. In the retroflection region of the North Brazilian Current (NBC) [*Richardson and Walsh*, 1986], maxima occur in August and out to September–October in the northeastern part of the plume. During the boreal winter and spring seasons, as the Amazon discharge level is low, the Amazon plume waters accumulate in the vicinity of the mouth due to northeastern trade wind events oriented roughly perpendicular to the coast [*Muller-Karger et al*., 1988, 1995; *Geyer et al*., 1996]. In late spring, as the discharge level increases, Amazon waters flow northwestward along the Brazilian shelf up to the Caribbean Sea when the wind relaxes and then reverses, to spread largely northwestward in May. In summer-early fall when the North Equatorial Counter Current develops, the river plume is carried eastward through the North Brazilian Current retroflection [*Muller-Karger et al*., 1988, 1995]. The plume starts to vanish northwestward in September and eastward in November. The maximum Amazon influence duration time (in months) is also analyzed (see Figure 4). Next to the mouth and northwestward along the Brazilian shelf, the influence is almost continuous between 10 and 12 months, as the plume is present in these areas almost all year long. The plume is only detected less than 6 months per year in general at the northern edges of the domain exhibiting high correlation between SMOS SSS and a_{cdm}.

4. Comparison Between SSS and a_{cdm} in the Amazon Plume

An illustration of results using different spatiotemporal sampling strategies is shown in Figure 5 for which the 25 km 10 day running mean SSS and a_{cdm} time series at location 1 ([6.5°N 46°W]) are represented. More

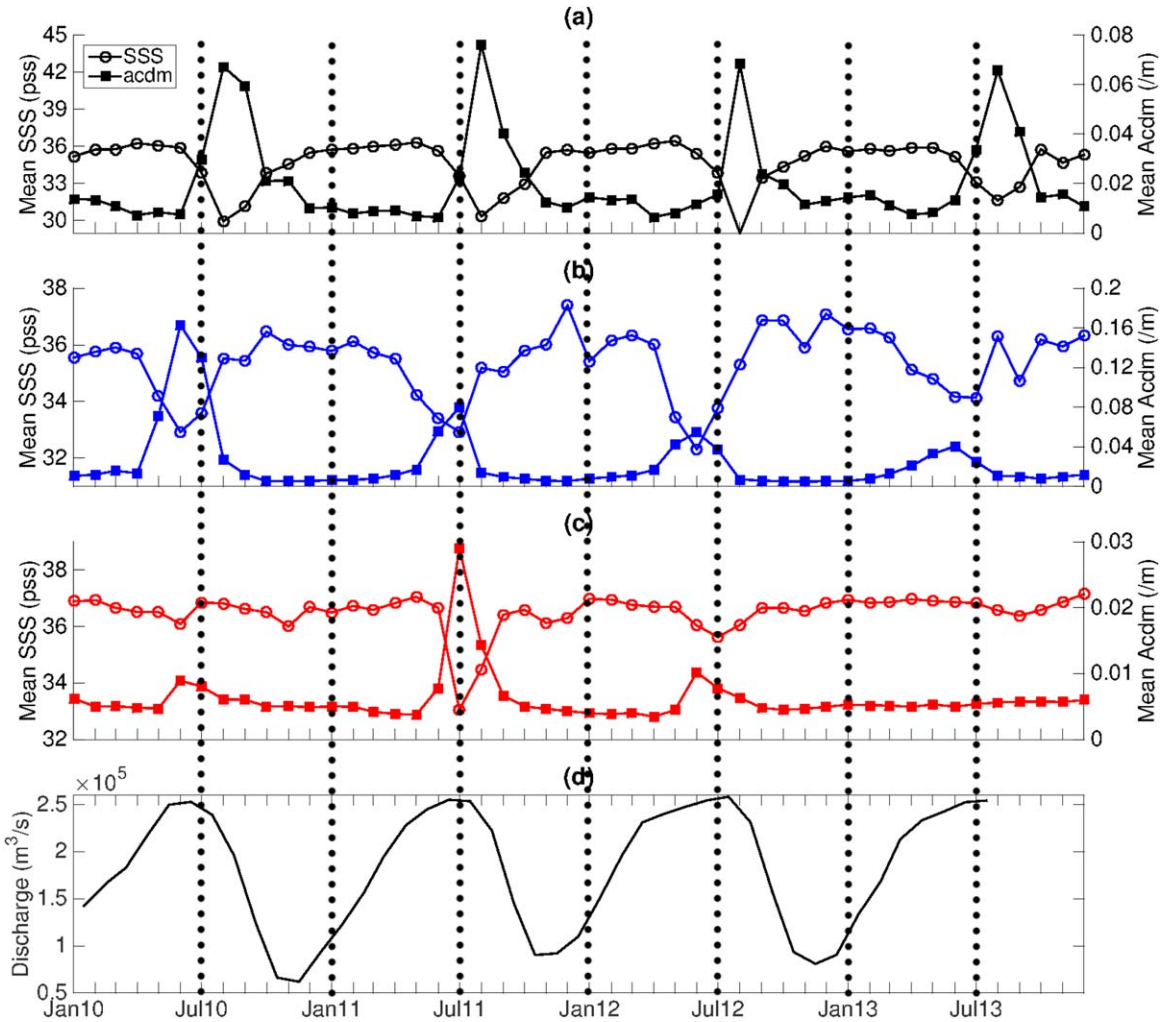

Figure 3. Time series of the monthly mean SMOS SSS (circles) and the monthly mean a_{cdm} (squares) computed at locations (a) 1, (b) 2, and (c) 3 shown on Figure 2; (d) time series of the monhtly Amazon discharge at Obidos gauge.

generally, for each 0.25 × 0.25° pixel, the 2010–2013 25 km 10 day running mean a_{cdm} and SMOS SSS signals exhibit a very strong overall anticorrelation with short-term fluctuations. As we are interested in the seasonal variations of SSS and a_{cdm} signals, both signals are first filtered using a time window ±45 days to get rid of high temporal variations (see Figure 5). This filter was selected to filter processes occurring at sub monthly time scales and to highlight those processes at seasonal scales. In this figure, the red solid line marks the maximum a_{cdm} occurence. In Figure 6, an example of the relationship between SSS and a_{cdm} is shown at location 1. The red solid line represents the linear regression over the filtered SMOS SSS and a_{cdm} time series (represented as black dots). We obtain a single linear relationship, robust for SSS > 30 pss ($R^2 = 0.92$). In this figure, we also provide the linear model reported by *Molleri et al.* [2010] (magenta). In Figure 7, the red solid line in each subplot represents the linear regression over the filtered SMOS SSS and a_{cdm} time series (represented as black dots) for each year 2010, 2011, 2012, and 2013. We also provide for each year, the relationship between daily ±5 days a_{cdm} and SSS (blue dots). For smaller SSS, corresponding to larger a_{cdm} values, clear variability is evidenced, mostly as a function of the different years of joint observations. Taking the linear regression evaluated with smoothed products, the map of the slope coefficient is further evaluated over the whole domain (see Figure 8). The slope significantly varies spatially, high in the northwestern part of the plume, around −0.025, to low in the eastern part of the plume and next to the mouth, around −0.005. To recall, Molleri and coauthors suggest a slope fixed at −0.008, which does not appear to be adequate to capture the natural variability of the salinity/a_{cdm} relationships. Amazon waters

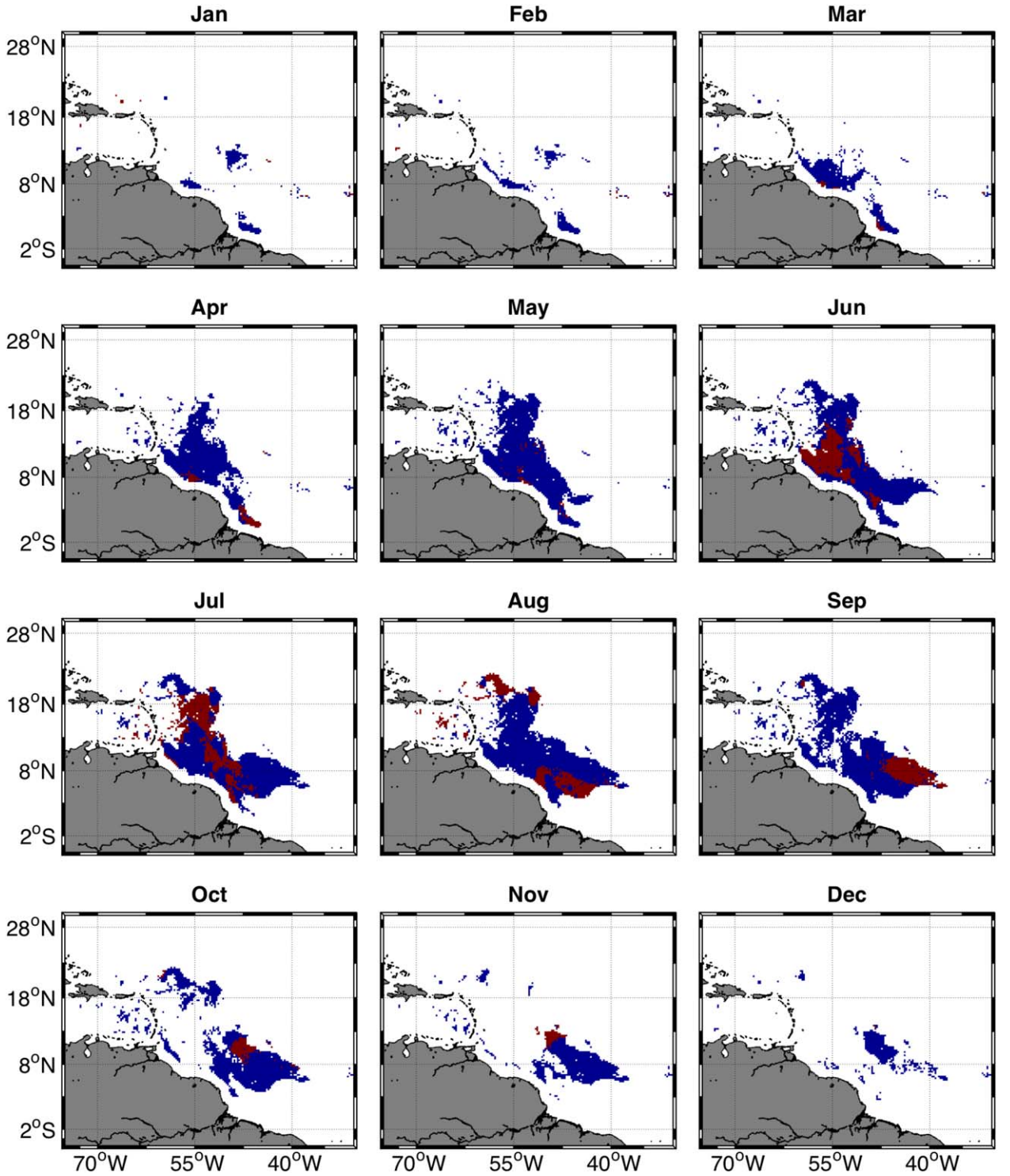

Figure 4. Seasonal evolution of the Amazon plume extension. Every month, the 0.25 × 0.25° pixels reached by the plume (months during which the a_{cdm} peak occurs for each pixel) are colored in blue. The pixels for which the time series extrema occurs in the current month are colored in red.

reaching the eastern part, during summer months, are fresh but apparently clearer (less absorption per pss) than the plume waters reaching the northwestern part of the plume. This could be due to removal processes that can affect the conservative mixing, these waters have generally been exposed to air-sea exchanges over longer periods and advected over larger distances from the source.

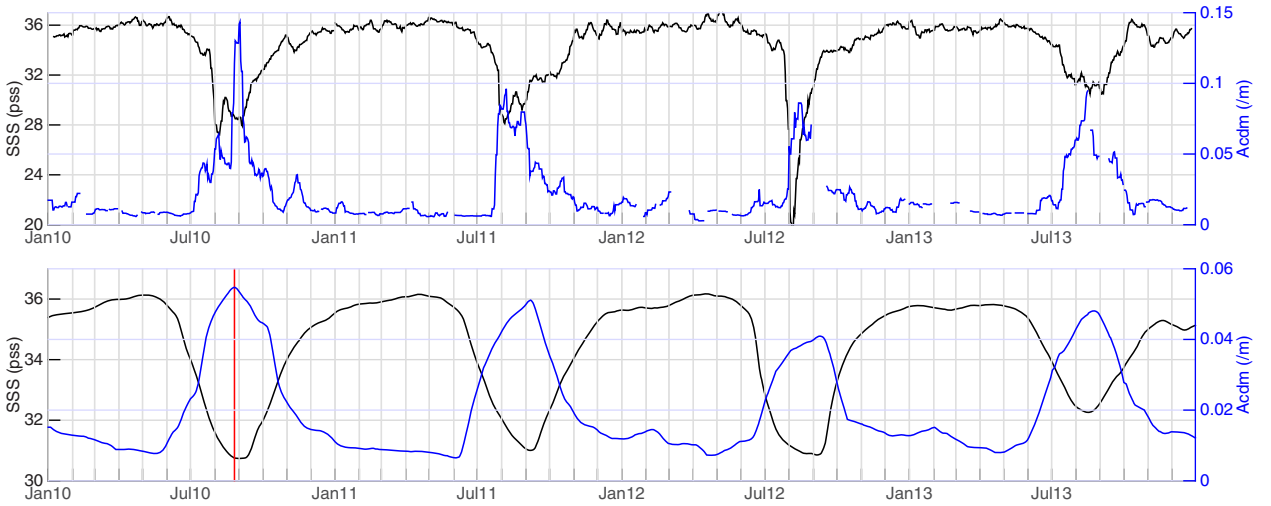

Figure 5. Time series of a_{cdm} (black) and SMOS SSS (blue) over 2010–2013 at location 1, 2, and 3 shown in Figure 2. On the top plot are represented the series at 10 days daily running mean temporal resolution, and on the bottom plot, the time series filtered using a daily ± 45 days. The red line marks the occurrence of the maximum of a_{cdm}.

5. Application

Applications of the conservative identity can be exploited for the reconstruction of a sea surface salinity product based on ocean color data. A benefit of this is the ability to estimate sea surface salinity back in time to correspond to the advent of ocean color data (e.g., 1997–2010 for NASA SeaWIFS). The spatial and temporal resolutions of ocean color sensors allow for interannual evaluations of plume dynamics. Moreover, using an adapted mean relationship helps to reveal anomalies to be possibly associated to biogeochemical optical properties and/or air-sea interaction variation [*Reul et al.*, 2013; *Grodsky et al.*, 2014]. Several examples have already been reported [*Binding and Bowers*, 2003; *Del Castillo and Miller*, 2008; *Molleri et al.*, 2010; *Urquhart et al.*, 2012; *Bai et al.*, 2013].

5.1. Methodology

We apply the linear regression between the 25 km daily ±45 days SMOS SSS and a_{cdm} computed for each 0.25 × 0.25° pixel in the Amazon plume over 2010–2013 (see Figure 8). Again, the regression was evaluated only for pixels in the plume for which the *p*-value (significance of the SSS-a_{cdm} correlation) is below 0.01 and the time lag between the SMOS SSS minimum and a_{cdm} maximum is zero. Then, from 25 km daily ±45 days a_{cdm} products, a 25 km daily ±45 days SSS product is retrieved.

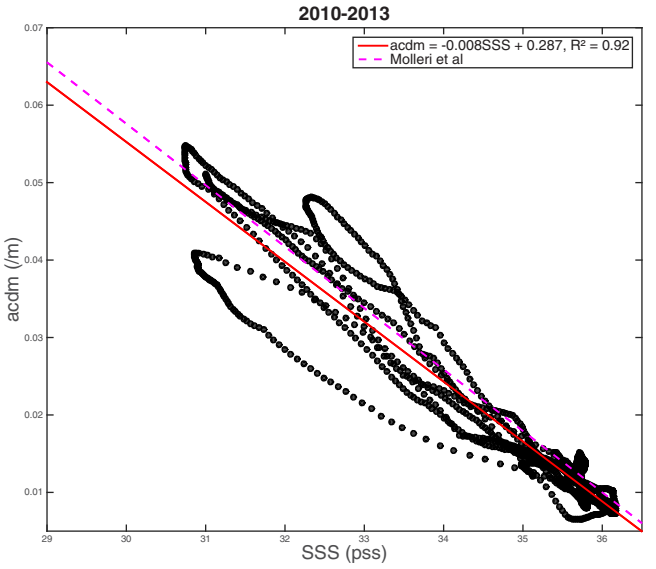

Figure 6. The 25 km 90 day running mean a_{cdm} as a function of 25 km 90 day running mean SMOS SSS over 2010–2013 (black dots) at location 1 shown in Figure 2. The red solid line represents the linear regression computed for that pixel over 2010–2013. The magenta dotted line represents the *Molleri et al.* [2010] linear model.

In parallel, we compute 25 km daily ±45 days SSS products retrieved using *Molleri et al.* [2010] and *Del Vecchio and Subramaniam* [2004] linear regression models, based on 25 km daily ±45 days a_{cdm} and K490, respectively.

5.2. Validation

We first assess the expected consistency of this ocean color-derived SSS with SMOS SSS over the 2010–2013 period and with in situ data over 2010–2012. In Figure 9, the evolution of the retrieved SSS is shown as a

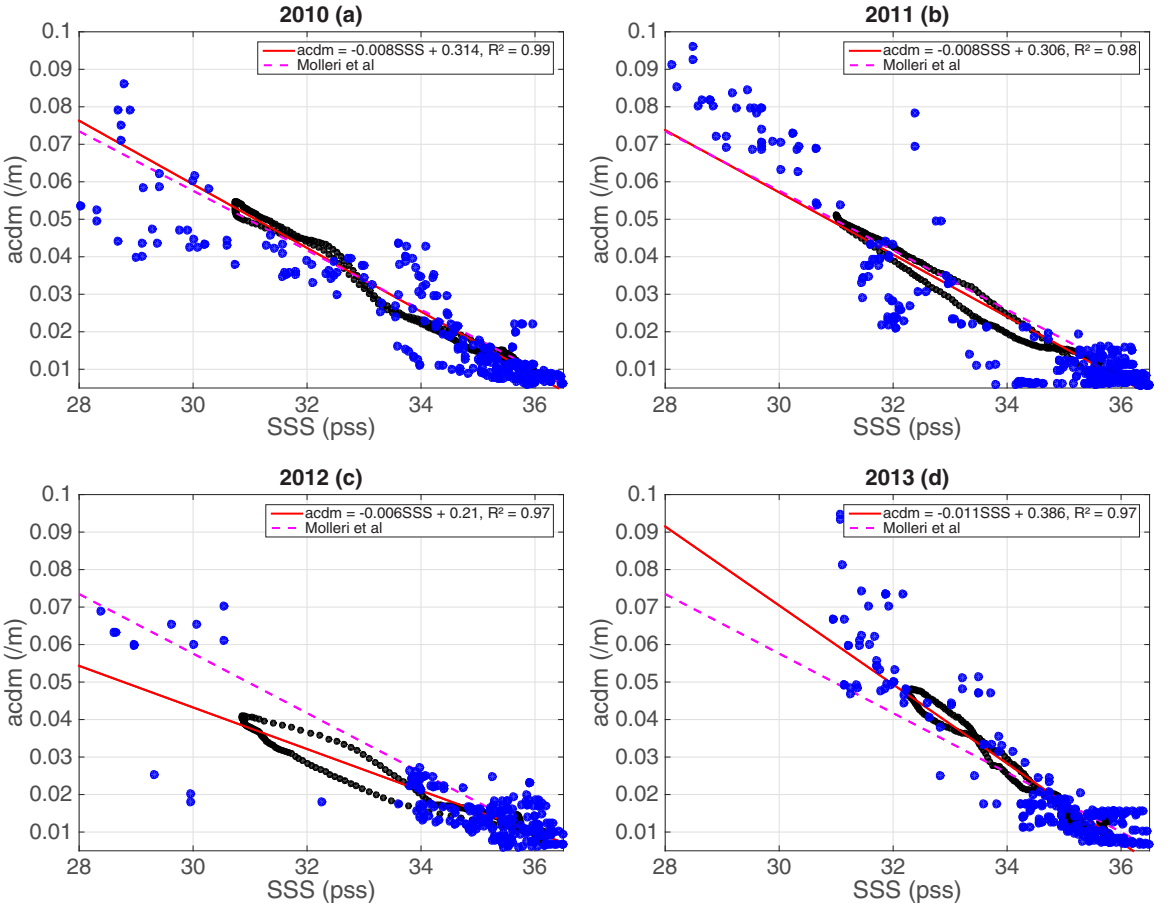

Figure 7. The 25 km 90 day running mean a_{cdm} as a function of 25 km 90 day running mean SMOS SSS in (a) 2010, (b) 2011, (c) 2012, and (d) 2013 (black dots) at location 1 shown in Figure 2. The red solid line represents the linear regression computed for that pixel for each year. The magenta dotted line represents the *Molleri et al.* [2010] linear model. The blue dots represent the 25 km 10 day running mean a_{cdm} as a function of 25 km 90 day running mean SMOS SSS in each year.

black solid line at the three particular locations 1, 2, and 3 (see Figure 2). The SMOS SSS evolution from 2010 is shown as a magenta solid line. In the eastern part of the plume, at location 1, the SSS agrees well in comparison with SMOS ($R^2 = 0.92$ (see Figure 6)). Low SSS waters differ at location 2 in the northwestern part of the plume (Rtern part of the plume, at location 1, the SSS agrees well in comparison with SMOS ($R^2 = 0.92$ and bias = 0.46 pss). Moreover, the SSS is not well retrieved for SSS higher than 35.5 pss. It corresponds to the plume limit where SSS and a_{cdm} no longer covary. There, at high SSS values, the a_{cdm} signal tied to salinity is weak. It has reached the open ocean value. At location 3, an area which is only reached by the plume in 2011, the marked SSS gradients are adequately retrieved ($R^2 = 0.77$ and bias = 0.18).

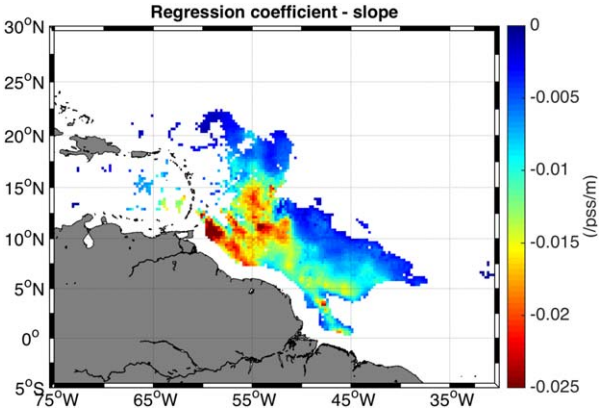

Figure 8. Slope of the linear regression between the time series of filtered SMOS SSS and a_{cdm} for each 0.25 × 0.25° pixel over 2010–2013. Only pixels in the plume for which the *p*-value (significance of the SSS-a_{cdm} correlation) is below 0.01 and time lag between the SMOS SSS minimum and a_{cdm} maximum is zero are shown.

For the three locations (see Figure 10), Hovmoller maps are provided to show the evolution of SMOS SSS and retrieved SSS from ocean color from 1998 to 2013. In each part of the plume, we identify the arrival of plume waters every year and the

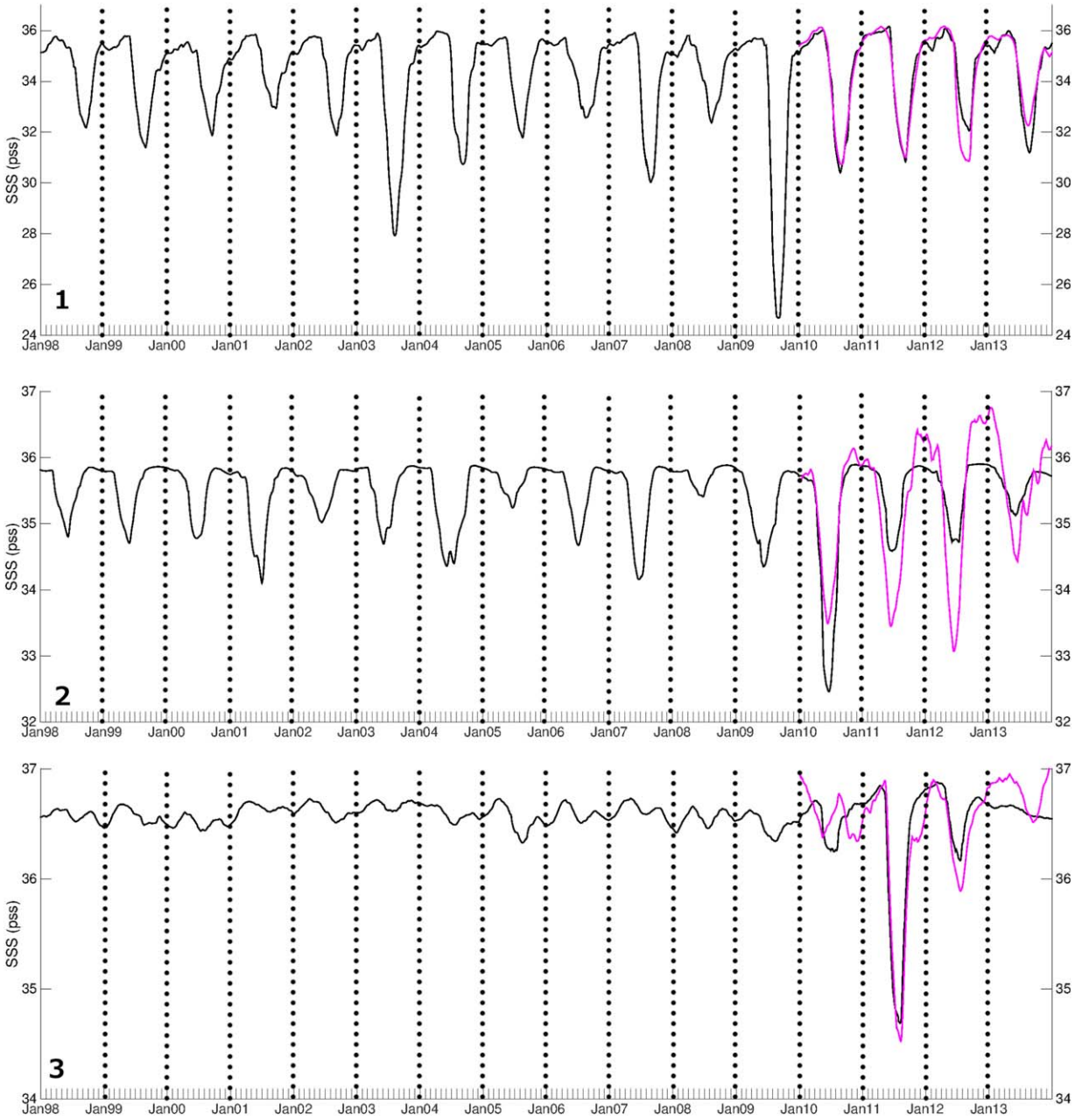

Figure 9. The 1998–2013 time series of retrieved SSS from ocean color (black) at locations 1, 2, and 3 shown in Figure 2. The magenta solid line represents the 2010–2013 time series of SMOS SSS.

variability in the extension of plume waters. An overall good agreement is noticed between the spatial extent of fresh and highly concentrated in organic matter pools spreading each year. In the eastern part of the plume (see Figure 11a), we can notice that in 2003 and 2009, the plume waters are carried further east than during other years, reaching 42°W. The Figure 11c shows the northeastern extension variability of the Amazon plume. As during most years, the plume does not reach 15°N in that part of the ocean in 2000, 2005, or 2010. The Amazon waters reach almost 17°N in 2011 and the plume extends further northeastward than other years, reaching 20°N. This shows that this new SSS product retrieved back in time from ocean color can be used to highlight, among others features, the interannual variability of the Amazon plume extension in order to relate it to other parameters (e.g., the discharge, precipitation, trade winds).

Retrieved SSS from ocean color is next compared to TSG transects in the Amazon plume. We show particularly the evolution of SSS along three different TSG tracks carried out in July and August 2010. Figure 12

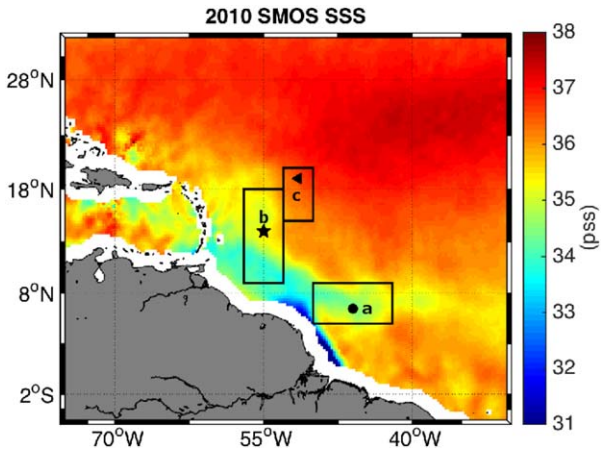

Figure 10. The 2010–2013 mean SMOS SSS on top of which are drawn the three boxes (a, b, and c) in which Hovm top of which are drawn (around locations 1, 2, and 3 shown in Figure 2).

shows the average July to August 2010 a_{cdm} on top of which are represented the TSG tracks crossing the Amazon plume, an area of strong SSS gradients. The retrieved SSS from ocean color using our regression model, *Molleri et al*. [2010] and *Del Vecchio and Subramaniam* [2004] models, SMOS SSS and in situ SSS along the three TSG tracks are represented as functions of the latitude in Figure 13. The strong SSS gradients, obtained when the ships cross the plume, are adequately retrieved by the different models. The *Molleri et al*. [2010] model tends to underestimate low SSS ($R^2 = 0.5$, $R^2 = 0.77$ and $R^2 = 0.63$ for each transect) whereas *Del Vecchio and Subramaniam* [2004] model tends to underestimate high SSS ($R^2 = 0.84$, $R^2 = 0.37$ and $R^2 = 0.49$ for each transect). As constructed, our model follows SMOS observations closely at high SSS. Low salinities retrievals are problematic, but overall agreement is clearly obtained ($R^2 = 0.84$, $R^2 = 0.91$ and $R^2 = 0.86$ for each transect).

At locations [7.75°N 50.75°W] and [8.75°N 50°W], labeled 4 and 5 in Figure 12, 1998–2013 time series of SMOS (magenta solid line) and retrieved SSS from ocean color (black solid line) are shown in Figure 14. At these two locations, in situ SSS data from *Colibri* and *Toucan* vessels are available from 2002 to 2013 and they are superposed as red dots on the time series. On the plot, we add the C-band and X-band brightness temperature differences from AMSR-E (blue solid line). *Reul et al*. [2009] already demonstrated that SSS in the Amazon plume region can be retrieved from space combining the vertically polarized C and X-bands brightness temperature (T_b) from AMSR-E. In warm waters, the SSS associated with the Amazon plume signal was shown to be clearly detectable using AMSR-E C and X-band T_b data, despite a much weaker sensitivity to SSS than the SMOS and Aquarius L-band sensors. The difference between the vertically polarized C and X-band T_bs estimated at the surface level is used in that method to isolate SSS signatures, minimizing the competing sea surface roughness and temperature impacts. For that purpose, we used the AMSR-E Level-1A T_b antenna data that were corrected for the atmospheric effects to estimate the C and X-band emission in vertical polarization from the ocean surface. These atmospheric corrections were evaluated using the radiative transfer model given by *Wentz and Meissner* [2000] applied to the coincident AMSR-E Level-2B water vapor, cloud liquid water, and sea surface wind products. In addition, the *Reynolds et al*., [2002] sea surface temperature products were used. The resulting surface reflectivities at each frequency were then combined to estimate the difference in surface brightness temperature between 6.9 and 10.7 GHz vertical polarization channels. At the two locations 4 and 5 shown in Figure 14, the spatial, seasonal, and interannual SSS variability seems well retrieved in the model SSS and in the AMSR-E T_bs difference compared to in situ and SMOS SSS (at these positions, rms < 1 pss between the model SSS and in situ SSS and between the model SSS and SMOS SSS).

6. Discussion

Retrieving SSS from ocean color based on the conservative mixing in the Amazon plume permits access to spaceborne SSS estimates back in time from 1998. Using this new product, the interannual and seasonal variability of the water plume dispersal in the northwestern tropical Atlantic Ocean using SSS as a tracer can be explored (see Figure 10). Thanks to spaceborne SSS measurement, a region north of the mouth reached by the Amazon plume waters only in summer 2011 has been highlighted. Moreover, using this new product as Amazon water plume tracer, we have demonstrated that in summer 2003 and 2009, the plume extended further north than during other years. This could be due to a change in currents and wind direction and speed or to more intense on land precipitation associated with the Inter Tropical Convergence Zone. Such processes can now be explored in depth and will undoubtedly aid in our understanding of air-atmosphere exchanges, especially regarding hurricane intensification [*Grodsky et al*., 2012].

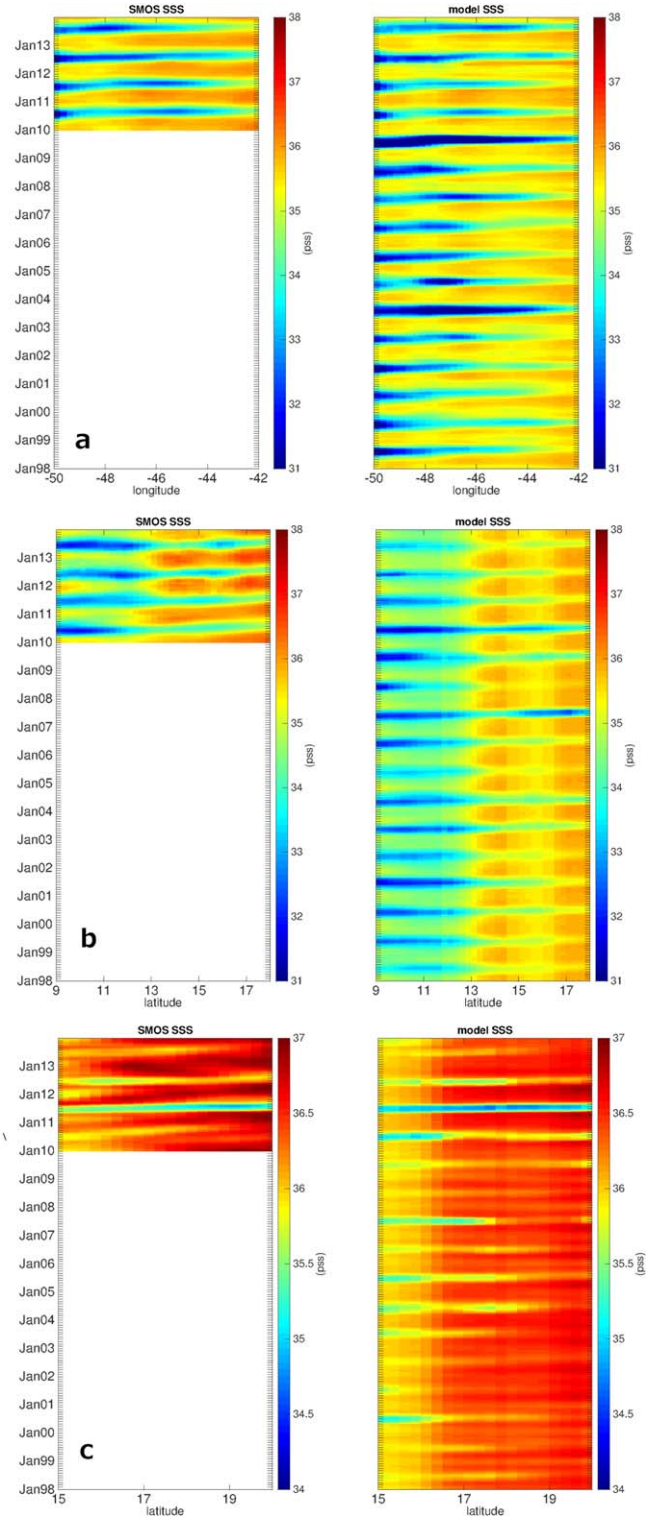

Figure 11. The 2010–2013 Hovmoller plots of (left) SMOS SSS, (middle) retrieved SSS from ocean color, and (right) a_{cdm} in the boxes a, b, and c represented in Figure 10.

Overall the method which retrieves SSS based on the conservative mixing established in this study shows good agreement with in situ data in comparison with methods based on conservative mixing relationship established in precedent studies (rms = 2.1 pss and bias = 1.2 pss for the current method; rms = 3 pss and bias = 1.7 pss for the *Molleri et al.* [2010] method; rms = 2 pss and bias = 1.5 pss for the *Del Vecchio and Subramaniam* [2004] method). However, different sources of error can impact in the retrieval of SSS based on ocean color products and the conservative mixing assumption. While validating SMOS SSS data against in situ data, discrepancies are noticeable, especially at low SSS (i.e., SSS < 30 pss). These discrepancies can be attributed to: (i) the high spatio-temporal variability of the SSS within the plume waters (horizontal and vertical variability). Horizontal and vertical SSS gradients in the Amazon plume region are strong (up to 7 pss over 50 km (SMOS resolution) and up to 3 pss/m). These gradients have a high variability in time and space that can be resolved by in situ instruments but not by SMOS. The discrepancies can also be attributed to (ii) potential errors in the satellite products in the proximity of land masses and/or when the radiometer data are contaminated by radio-frequency interferences (RFI); (iii) potential errors in the dielectric constant model used in the SSS retrieval algorithm; (iv) eventual issues in the L3 SMOS SSS products correction based on climatologic SSS data; (v) differences in the respective spatio-temporal sampling characteristics of the space and in situ sensors [*Boutin et al.*, 2012; *Reul et al.*, 2012; *Font et al.*, 2013]. The validation against in situ data is based on a comparison between data acquired at a precise time and location and data averaged over 43 km. This spatial and temporal difference can impact the comparisons. Moreover, in situ data are often measured at around 3 or 5 m deep, whereas spaceborne instruments measure only the first few centimeters of the ocean. In the Amazon plume area, vertical SSS gradients can certainly be large.

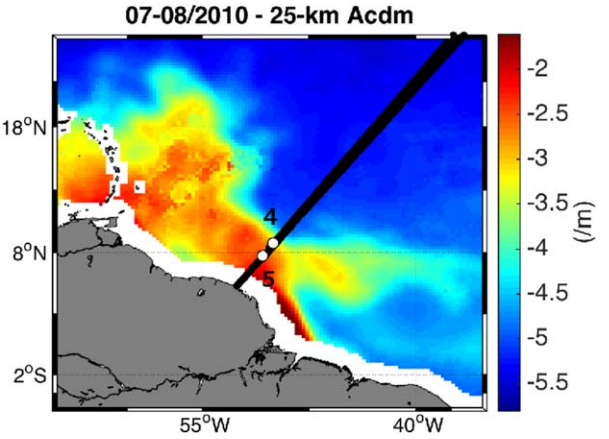

Figure 12. Average July to August 2010 a_{cdm} map on top of which are represented as solid black lines, three TSG transects. The white dots, labeled 4 and 5, mark the locations [7.75°N 50.75°W] and [8.75°N 50°W].

Near the coast, where turbid waters are present, a_{cdm} retrieval algorithms may also not be precise enough, inducing additional errors in the model. In addition to its role as a tracer of freshwater in coastal regions, colored detrital matter contributes to total light attenuation in the blue region of the spectrum where chlorophyll-a also absorbs strongly. This can lead to large errors in ocean color retrievals.

Deviations from the conservative mixing can occur due to biogeochemical processes such as primary production and removal processes. Photolysis or photo-oxidation, the degradation of the cdm mainly due to irradiance exposure, is one of the possible removal processes that can affect the conservative mixing. Riverine light absorbing materials are highly concentrated in the waters discharged by the Amazon River and this can attenuate light penetration and reflectance. At the edges of the plume, where the riverine materials have less impact on the optical field, light will penetrate deeper where it can degrade optically active riverine constituents. Primary productivity may also add cdm to the pool (source of cdm) disrupting the conservative mixing relationship between cdm and salinity. Indeed, in late summer, the

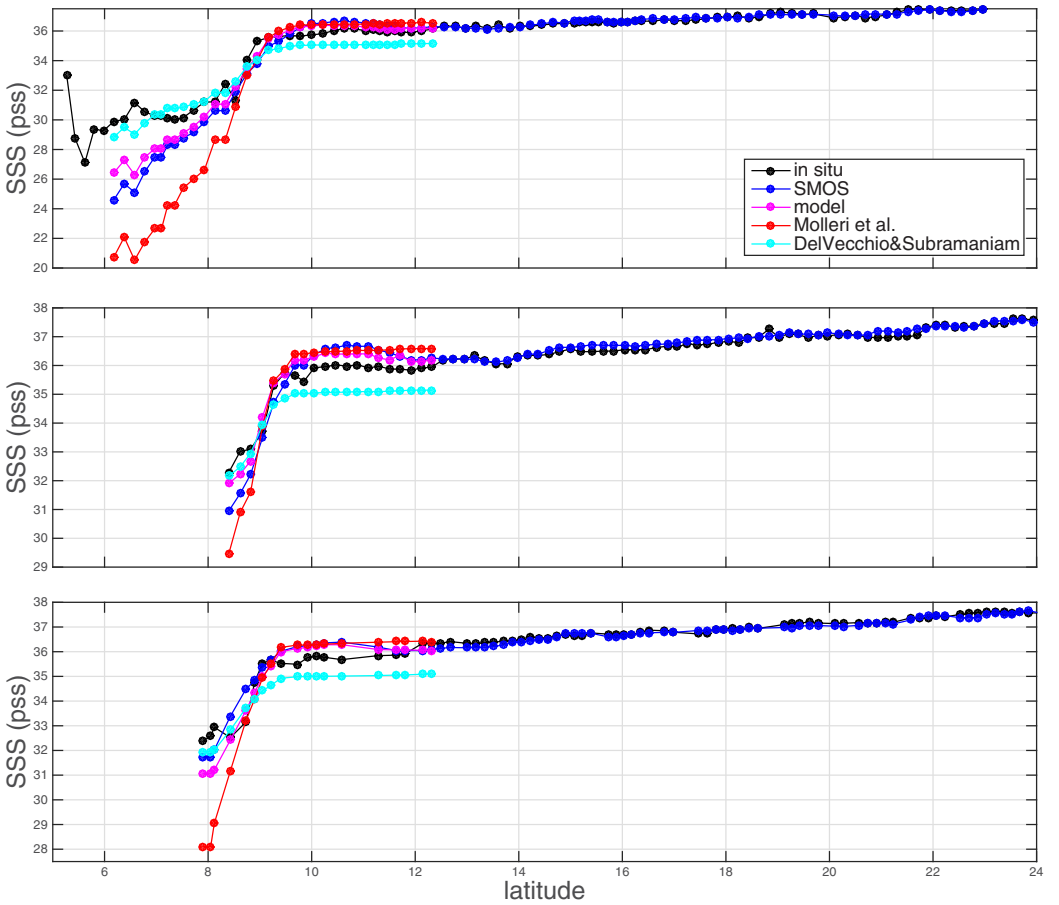

Figure 13. Transects of sea surface salinity from SMOS (blue dots), retrieved SSS from ocean color using our model (magenta dots), using *Del Vecchio and Subramaniam* [2004] model (cyan dots) and using *Molleri et al.* [2010] model (red dots) and TSG SSS measurements (black dots) along three TSG transects in July and August 2010.

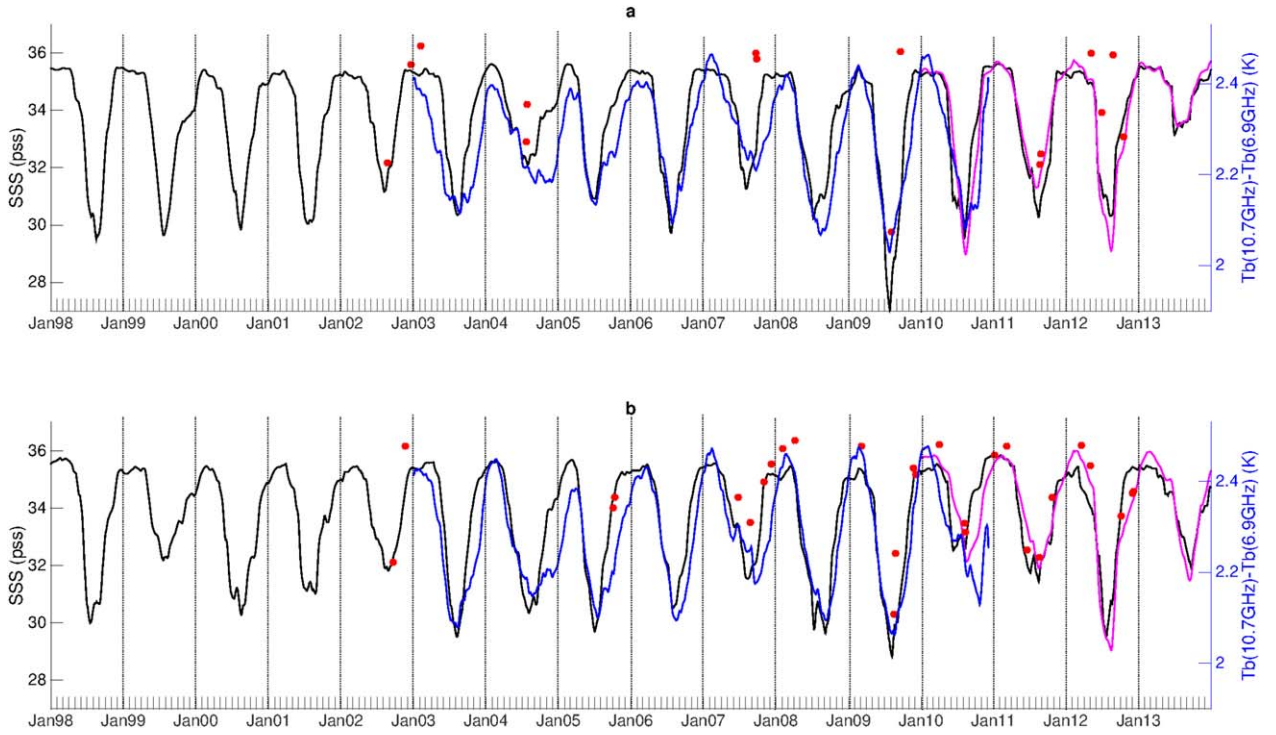

Figure 14. The 1998–2013 time series of retrieved SSS from ocean color (black) at locations 4 and 5 shown in Figure 12. The magenta solid line represents the 2010–2013 time series of SMOS SSS. The blue line represents the AMSR-E ΔTb time series from 2003 to 2010 rescaled to match the SSS scale. The red dots represent in situ data available.

arrival of nutrient-rich Amazon River waters often stimulates primary production and thus can induce an increase of dissolved organic matter next to the Caribbean Sea [*Beers et al*., 1968]. In summer, from May to July, biological activity increases in the northwestern part of the plume. This is evident in monthly maps of primary productivity (not shown here) computed using the CbPM data [*Westberry et al*., 2008] showing intense regional productivity [also see *Salisbury et al*., 2011]. Thus, errors may have been introduced when computing the conservative mixing in each pixel over the years 2010–2013 (at location 2, bias = 0.5 pss and at location 1 and 3 respectively, bias = 0.3 pss and bias = 0.1 pss). During that time, high interannual variability hinders a determination of simple relationships for low SSS and high colored detrital matter absorption. Figure 15 presents the relationship between a_{cdm} and SSS. A deviation from conservative mixing is clearly visible in 2010 associated with unusually large values of CbPM net primary production estimates.

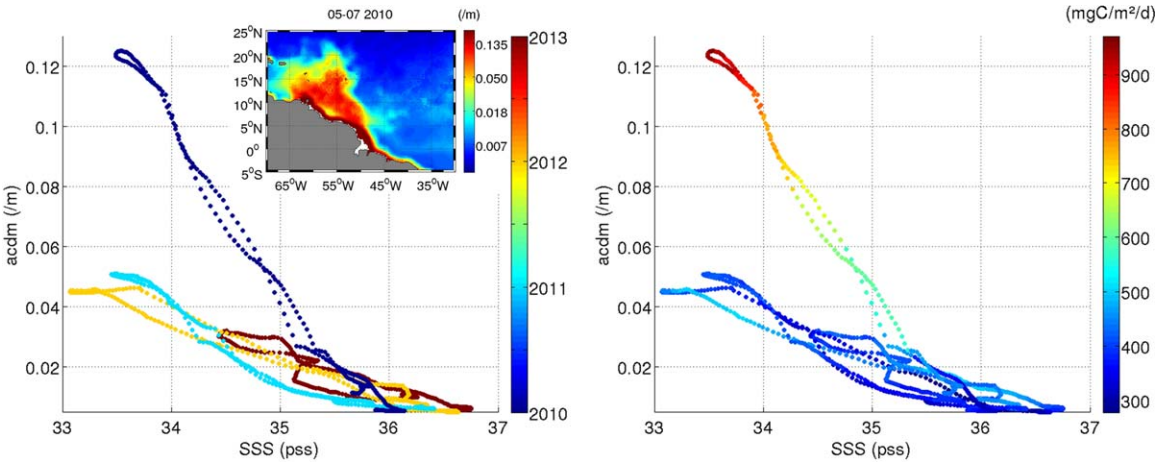

Figure 15. The 25 km 90 day a_{cdm} versus SMOS SSS at location 3 ([14°N, 55°W]) pointed out by a black dot on the May through July average a_{cdm} map. The *z* axis represents (left) the year of observation and (right) the CbPM net primary productivity from Ocean Productivity.

7. Conclusion

This study documents the relationship between sea surface salinity and optical parameters using spaceborne SSS and ocean color data in the Amazon plume. The consistency between a microwave instrument and optical instruments is clearly demonstrated. This represents a new potential for the study of the SSS-a_{cdm} relationship with a largely improved spatiotemporal monitoring compared to approaches that rely on in situ data.

Throughout the year Amazon waters are advected from the mouth to the open ocean and mix with the surrounding water masses. At a fixed location, Amazon waters reach each region of the plume periodically through different advection pathways and after encountering different water masses. With satellite observations the conservative mixing model can then be more locally applied for each $0.25 \times 0.25^{\circ}$ pixel in the plume area. The conservative mixing relationship is then mapped to follow space-time characteristics including seasonal scales of variability. Accordingly, these first results invite further ocean color-surface salinity comparisons. More specifically, the apparent robustness of the use of the K490 parameter in low-salinity waters necessitates further investigations closer to the coast.

The robustness of the relationship between a_{cdm} and surface salinity varies depending on where and when the parameterization is calculated. Clear interannual and space variabilities in the SSS-a_{cdm} relationship have been highlighted. This has important biogeochemical implications for marine biology and carbon cycle science. Our results suggest that for accurate salinity retrievals using ocean color data multiple parameterizations distributed in time and/or space are required. A particular high slope field or end-member does not always coincide with the highest correlation field. Biogeochemical removal or production mechanisms, in addition to the difficulties of working with satellite data in near-coastal region are factors requiring characterization.

Once the conservative mixing relationships were established, a daily $\pm$45 days 25 km SSS product based on ocean color data is retrieved. This product is validated against SMOS and in situ SSS and compared with the SSS retrieved from ocean color using the *Molleri et al*. [2010] and *Del Vecchio and Subramaniam* [2004] models. Generally, the proposed model yields good results especially for SSS $>$ 30 pss and SSS $<$ 36 pss (rms = 1.9 pss and bias = 1.2 pss). At low SSS (SSS $<$ 30 pss), the present model tends to overestimate SSS (bias of 4 pss for SSS$<$30 pss).

Acknowledgments

This work was partly performed under ESA contract ESA/ESRIN/RFQ/3-12269/08/I-LGSMOS, and with support from CNES in the context of development of the Expert Support Laboratory of the Centre Aval de Traitement des Données SMOS (CATDS) and from NASA's Physical Oceanography program grant NNX13AE19G and NASA OBB NNX08AL80G and NNX13AM38G. Data for this paper are available at the following data centers we gratefully thank: the Ocean Salinity Expertise Center (CECOS) of the CNES-IFREMER Centre Aval de Traitement des Donnees SMOS (CATDS) (http://catds.ifremer.fr) for SMOS SSS data; ACRI-ST GlobColour service (http://www.globcolour.info/) for ocean color data; NOAA Physical Oceanography Division (PHOD) of AOML (http://www.aoml.noaa.gov/) and Coriolis processing center (http://www.coriolis.eu.org) for in situ observations; Environmental Research Observatory Geodynamical, hydrological and biogeochemical control of erosion/alteration and material transport in the Amazon basin (ORE-HYBAM) (http://www.ore-hybam.org/) for discharge levels measurements; Ocean Productivity (http://www.science.oregonstate.edu/ocean.productivity/) for NPP data; and the National Snow and Ice Data Center (NSIDC) (http://nsidc.org/data/) for AMSR-E brightness temperature data. We thank the reviewers for their constructive comments and corrections.

References

Bai, Y., D. Pan, W.-J. Cai, X. He, D. Wang, B. Tao, and Q. Zhu (2013), Remote sensing of salinity from satellite-derived CDOM in the Changjiang river dominated east China sea, *J. Geophys. Res. Oceans*, *118*, 227–243, doi:10.1029/2012JC008467.

Battin, T. J. (1998), Dissolved organic matter and its optical properties in a blackwater tributary of the upper Orinoco river, *Venezuela, Org. Geochem.*, *28*(9-10), 561–569.

Baumgartner, A., and E. Reichel (1975), *The World Water Balance*, University of California, 179 pp., Elsevier.

Beers, J. R., D. M. Steven, and J. B. Lewis (1968), Primary productivity in the Caribbean sea off Jamaica and the tropical north Atlantic off Barbados, *Bull. Mar. Sci.*, *18*(1), 86–104.

Binding, C., and D. Bowers (2003), Measuring the salinity of the Clyde Sea from remotely sensed ocean colour, *Estuarine Coastal Shelf Sci.*, *57*(4), 605–611.

Blough, N., and R. Del Vecchio (2002), Chromophoric DOM in the coastal environment, in *Biogeochemistry of Marine Dissolved Organic Matter*, edited by D. E. A. E. Hansell, pp. 509–546. Elsevier, Academic, San Diego, Calif.

Boutin, J., N. Martin, X. Yin, J. Font, N. Reul, and P. Spurgeon (2012), First assessment of SMOS data over open ocean: Part II—Sea surface salinity, *IEEE Trans. Geosci. Remote Sens.*, *50*(5), 1662–1675.

Bowers, D., and H. Brett (2008), The relationship between CDOM and salinity in estuaries: An analytical and graphical solution, *J. Mar. Syst.*, *73*(1-2), 1–7.

Chen, Z., C. Hu, R. N. Conmy, F. Muller-Karger, and P. Swarzenski (2007), Colored dissolved organic matter in Tampa bay, *Florida, Mar. Chem.*, *104*(1-2), 98–109.

Del Castillo, C. E., and R. L. Miller (2008), On the use of ocean color remote sensing to measure the transport of dissolved organic carbon by the Mississippi river plume, *Remote Sens. Environ.*, *112*(3), 836–844.

Del Vecchio, R., and A. Subramaniam (2004), Influence of the Amazon river on the surface optical properties of the western tropical north Atlantic ocean, *J. Geophys. Res.*, *109*, C11001, doi:10.1029/2004JC002503.

Ferrari, G., and M. Dowell (1998), CDOM absorption characteristics with relation to fluorescence and salinity in coastal areas of the southern Baltic sea, *Estuarine Coastal Shelf Sci.*, *47*(1), 91–105.

Ferry, N., and G. Reverdin (2004), Sea surface salinity interannual variability in the western tropical Atlantic: An ocean general circulation model study, *J. Geophys. Res.*, *109*, C05026, doi:10.1029/2003JC002122.

Font, J., et al. (2013), SMOS first data analysis for sea surface salinity determination, *Int. J. Remote Sens.*, *34*(9-10), 3654–3670.

Fournier, S. (2014), Spatio-temporal coherence between spaceborne measurements of salinity and optical properties in the Amazon-Orinoco Plume region, PhD thesis, Ifremer, Brest, France.

Fratantoni, D. M., and D. A. Glickson (2002), North Brazil current ring generation and evolution observed with Sea WiFS, *J. Phys. Oceanogr.*, *32*(3), 1058–1074.

Geyer, W. R., R. C. Beardsley, S. J. Lentz, J. Candela, R. Limeburner, W. E. Johns, B. M. Castro, and I. D. Soares (1996), Physical oceanography of the Amazon shelf, *Cont. Shelf Res.*, *16*(5-6), 575–616.

Granskog, M. A., R. W. Macdonald, C.-J. Mundy, and D. G. Barber (2007), Distribution, characteristics and potential impacts of chromophoric dissolved organic matter (CDOM) in Hudson strait and Hudson bay, Canada, *Cont. Shelf Res.*, *27*(15), 2032–2050.
Grodsky, S. A., N. Reul, G. Lagerloef, G. Reverdin, J. A. Carton, B. Chapron, Y. Quilfen, V. N. Kudryavtsev, and H.-Y. Kao (2012), Haline hurricane wake in the Amazon/Orinoco plume: AQUARIUS/SACD and SMOS observations, *Geophys. Res. Lett.*, *39*, L20603, doi:10.1029/2012GL053335.
Grodsky, S. A., G. Reverdin, J. A. Carton, and V. J. Coles (2014), Year-to-year salinity changes in the Amazon plume: Contrasting 2011 and 2012 Aquarius/SACD and SMOS satellite data, *Remote Sens. Environ.*, *140*, 14–22.
Hickey, B. M., et al. (2010), River influences on shelf ecosystems: Introduction and synthesis, *J. Geophys. Res.*, *115*, C00B17, doi:10.1029/2009JC005452.
Hu, C., F. E. Muller-Karger, D. C. Biggs, K. L. Carder, B. Nababan, D. Nadeau, and J. Vanderbloemen (2003), Comparison of ship and satellite bio-optical measurements on the continental margin of the NE gulf of Mexico, *Int. J. Remote Sens.*, *24*(13), 2597–2612.
Hu, C., E. T. Montgomery, R. W. Schmitt, and F. E. Muller-Karger (2004), The dispersal of the Amazon and Orinoco River water in the tropical Atlantic and Caribbean Sea: Observation from space and S-PALACE floats, *Deep Sea Res.*, Part II, *51*, 1151–1171.
Huang, W., and R. F. Chen (2009), Sources and transformations of chromophoric dissolved organic matter in the Neponset river watershed, *J. Geophys. Res.*, *114*, G00F05, doi:10.1029/2009JG000976.
Körtzinger, A. (2003), A significant CO_2 sink in the tropical Atlantic ocean associated with the Amazon river plume, *Geophys. Res. Lett.*, *30*(24), 2287, doi:10.1029/2003GL018841.
Lentz, S. J. (1995), Seasonal variations in the horizontal structure of the Amazon plume inferred from historical hydrographic data, *J. Geophys. Res.*, *100*(C2), 2391–2400.
Lentz, S. J., and R. Limeburner (1995), The Amazon river plume during AMASSEDS: Spatial characteristics and salinity variability, *J. Geophys. Res.*, *100*(C2), 2355–2375.
Longhurst, A. (1995), Interpreting CZCS images of the Amazon plume: Reply, *Deep Sea Res.*, Part I, *42*(11–12), 2139–2141.
Maritorena, S., D. A. Siegel, and A. R. Peterson (2002), Optimization of a semianalytical ocean color model for global-scale applications, *Appl. Opt.*, *41*(15), 2705–2714.
Masson, S., and P. Delecluse (2001), Influence of the Amazon river runoff on the tropical Atlantic, *Phys. Chem. Earth, Part B*, *26*(2), 137–142.
McKee, B., R. Aller, M. Allison, T. Bianchi, and G. Kineke (2004), Transport and transformation of dissolved and particulate materials on continental margins influenced by major rivers: Benthic boundary layer and seabed processes, *Cont. Shelf Res.*, *24*(7–8), 899–926.
Meybeck, M., and A. Ragu (1997), River Discharges to the Oceans: An Assessment of Suspended Solids, *Major Ions, and Nutrients*, *243* pp., IASH, Université Pierre et Marie Curie, Paris, France.
Mignot, J., A. Lazar, and M. Lacarra (2012), On the formation of barrier layers and associated vertical temperature inversions: A focus on the northwestern tropical Atlantic, *J. Geophys. Res.*, *117*, C02010, doi:10.1029/2011JC007435.
Miller, W. L., and R. G. Zepp (1995), Photochemical production of dissolved inorganic carbon from terrestrial organic matter: Significance to the oceanic organic carbon cycle, *Geophys. Res. Lett.*, *22*(4), 417–420.
Molleri, G. S., E. M. de M. Novo, and M. Kampel (2010), Space-time variability of the Amazon river plume based on satellite ocean color, *Cont. Shelf Res.*, *30*(3–4), 342–352.
Moran, M., W. Sheldon, and J. Sheldon (1999), Biodegradation of riverine dissolved organic carbon in five estuaries of the southeastern United States, *Estuaries*, *22*(1), 55–64.
Muller-Karger, F., C. McClain, and P. Richardson (1988), The dispersal of the Amazon's water, *Nature*, *333*(6168), 56–59.
Muller-Karger, F., P. Richardson, and D. Mcgillicuddy (1995), On the offshore dispersal of the Amazon's plume in the north Atlantic: Comments on the paper by A. Longhurst, " Seasonal cooling and blooming in tropical oceans", *Deep Sea Res.*, Part I, *42*(11–12), 2127–2137.
Obernosterer, I., and G. J. Herndl (2000), Differences in the optical and biological reactivity of the humic and non-humic DOC component in two contrasting coastal marine environments, *Limnol. Oceanogr.*, *45*, 1120–1129.
Pailler, K., B. Bourlès, and Y. Gouriou (1999), The barrier layer in the western tropical Atlantic ocean, *Geophys. Res. Lett.*, *26*(14), 2069–2072.
Reul, N., S. Saux-Picart, B. Chapron, D. Vandemark, J. Tournadre, and J. Salisbury (2009), Demonstration of ocean surface salinity microwave measurements from space using AMSR-E data over the Amazon plume, *Geophys. Res. Lett.*, *36*, L13607, doi:10.1029/2009GL038860.
Reul, N., J. Tenerelli, J. Boutin, B. Chapron, F. Paul, E. Brion, F. Gaillard, and O. Archer (2012), Overview of the first SMOS sea surface salinity products. Part I: Quality assessment for the second half of 2010, *IEEE Trans. Geosci. Remote Sens.*, *50*(5), 1636–1647.
Reul, N., et al. (2013), Sea surface salinity observations from space with the SMOS satellite: A new means to monitor the marine branch of the water cycle, *Surv. Geophys.*, *35*, 681–722.
Reynolds, R. W., N. A. Raynar, T. M. Smith, D. C. Stokes, and W. Wanqiu (2002), An improved in situ satellite SST analysis for climate, *J. Clim.*, *15*(13), 1609–1625.
Richardson, P. L., and D. Walsh (1986), Mapping climatological seasonal variations of surface currents in the tropical Atlantic using ship drifts, *J. Geophys. Res.*, *91*(C9), 10,537–10,550.
Salisbury, J., D. Vandemark, J. Campbell, C. Hunt, D. Wisser, N. Reul, and B. Chapron (2011), Spatial and temporal coherence between Amazon river discharge, salinity, and light absorption by colored organic carbon in western tropical Atlantic surface waters, *J. Geophys. Res.*, *116*, C00H02, doi:10.1029/2011JC006989.
Salisbury, J. E. (2003), Satellite indices of fluvial influence in coastal waters, PhD thesis, Nat. Resour. and Earth Syst. Sci., Univ. of N. H., Durham, N. H.
Salisbury, J. E., D. Vandemark, C. W. Hunt, J. W. Campbell, W. R. McGillis, and W. H. McDowell (2008), Seasonal observations of surface waters in two Gulf of Maine estuary-plume systems: Relationships between watershed attributes, optical measurements and surface p CO_2, *Estuarine Coastal Shelf Sci.*, *77*(2), 245–252.
Tomczak, M. (1999), Some historical, theoretical and applied aspects of quantitative water mass analysis, *J. Mar. Res.*, *57*(2), 275–303.
Twardowski, M. S., and P. L. Donaghay (2001), Separating in situ and terrigenous sources of absorption by dissolved materials in coastal waters, *J. Geophys. Res.*, *106*(C2), 2545–2560.
Urquhart, E. A., B. F. Zaitchik, M. J. Hoffman, S. D. Guikema, and E. F. Geiger (2012), Remotely sensed estimates of surface salinity in the Chesapeake bay: A statistical approach, *Remote Sens. Environ.*, *123*, 522–531.
Wentz, F., and T. Meissner (2000), *AMSR-E Ocean Algorithm*, *Algorithm Theoretical Basis Document*, *Version 2*, Remote Sens. Syst., Santa Rosa, Calif.
Westberry, T., M. J. Behrenfeld, D. A. Siegel, and E. Boss (2008), Carbon-based primary productivity modeling with vertically resolved photoacclimation, *Global Biogeochem. Cycles*, *22*, GB2024, doi:10.1029/2007GB003078.
Yamashita, Y., and E. Tanoue (2004), In situ production of chromophoric dissolved organic matter in coastal environments, *Geophys. Res. Lett.*, *31*, L14302, doi:10.1029/2004GL019734.